A Learning-Based Sensor Array for Untethered Soft Prosthetic Hand Aiming at Restoring Tactile Sensation

Haipeng Xu, Yu Rong, Jieji Ren, Ningbin Zhang, Yi Zhao, Xinyu Yang, Zhenpu Zhu, and Guoying Gu*

Endowing tactile feedback for prosthetic hands is profound for upper-limb amputees. However, existing prosthetic hands are generally not in possession of the embedded sensory feedback. Herein, a flexible tactile sensor array which can be integrated into an untethered soft prosthetic hand to achieve static and dynamic discrimination tasks is presented. The flexible piezoresistive sensory arrays with 25 sensor units which can be arranged on five fingers of the soft prosthetic hand are fabricated. According to the collected large-scale tactile dataset (including pressure distribution and pressure magnitude) during different grasping tasks, a learning-based classification model that can reveal the correspondences between tactile information and object attributes while interacting with touched objects is developed. To transfer tactile information extracted from tactile sensor arrays, a wearable vibrotactile feedback band with a spatial coding feedback strategy is implemented by selectively activating vibrotactile motors located on the skin of the upper arm. In a set of tests performed by an individual with transradial amputation and eight able-bodied subjects, the soft prosthetic hand integrated with tactile sensor arrays can help the users regain finger tactile sensation, discriminate grasped objects, and achieve real-time dynamic rolling detection.

1. Introduction

The dexterous operation of human hands, combined with the sophisticated sense of touch, plays a vital role in interacting with surroundings and feeling the world.[1–3] The loss of the hand seriously limits the person's ability in daily life.[4–7] The use of prosthetic hands is proven to be a viable option for replicating the appearance and motor function of missing hands for individuals with upper-limb amputation.[3,4,8–10] During past decades, many anthropomorphic prosthetic hands have been commercialized to provide dexterous grasping functionality (such as the Vincent hand, the i-Limb hand, the Bebionic hand, and the Michelangelo hand), which are capable of achieving both power grasping of heavy objects and delicate manipulation.[11–14] However, these existing prosthetic hands generally fail to restore tactile sensation and sensory feedback. Consequently, amputees using hand prostheses usually complain during daily use.[6,15–17] The gaps and challenges mainly lie in: 1) designing and integrating tactile sensor arrays for prosthetic hands to detect rich touch information without hindering the motor function and portability of hand prostheses;[8,18,19] and 2) encoding and transferring the sensory information to the user in real time with high ease of wearing.[15,20] Hence, it remains elusive to integrate tactile sensors and wearable feedback device into an untethered prosthetic hand.

Recently, with the development of soft robotics,[21–23] various soft tactile sensors with different sensing principles such as resistive,[24–26] capacitive,[27–29] triboelectric,[30,31] magnetic,[32,33] and optoelectronic[34,35] have been developed to mimic functions of human receptors. Remarkable sensing capability such as high sensitivity,[36–38] low hysteresis,[39,40] low detection limit,[41,42] and high array density[43,44] have been reported to further facilitate perceptive functions. Although these available sensors perform fairly well at some specific tasks to capture information about force, strain, and torque, few of them are able to be integrated into the prosthetic hand due to the mismatch of mechanical properties and bulky measuring instruments.[45] On the other hand, sensory feedback is important to improve grasping capability[46] and decrease cognitive effort.[47–49] Groundbreaking results show that invasive implanted peripheral nerve electrodes[15,50] can successfully help amputees regain touch sensation. Due to the complexity of invasive surgical procedures, sensory substitution through noninvasive methods (such as electrotactile and vibrotactile) has been a promising alternative.[20,51,52] Remapping the sensor's response with an encoding strategy

H. Xu, Y. Rong, J. Ren, N. Zhang, Y. Zhao, X. Yang, Z. Zhu, G. Gu
Robotics Institute
School of Mechanical Engineering
Shanghai Jiao Tong University
Shanghai 200240, China
E-mail: guguoying@sjtu.edu.cn

H. Xu, Y. Rong, J. Ren, N. Zhang, Y. Zhao, X. Yang, Z. Zhu, G. Gu
State Key Laboratory of Mechanical System and Vibration
Shanghai Jiao Tong University
Shanghai 200240, China

**ADVANCED
SCIENCE NEWS**
www.advancedsciencenews.com

**ADVANCED
INTELLIGENT
SYSTEMS**
Open Access
www.advintellsyst.com

through the feedback device to convey grasping information can further improve the utility of the hand prosthesis such as controlling of the grasping force.[20,53]

In this article, flexible piezoresistive tactile sensor arrays are proposed for enhancing the sensing intelligence of the untethered soft prosthetic hand, as shown in **Figure 1**a. The developed tactile sensor arrays with 25 sensor units can be uniformly arranged on five fingers of the soft prosthetic hand to measure the touch pressure. To verify its sensing capability, a series of tests are performed to demonstrate the sensitivity and durability of the tactile sensor arrays. After integrating tactile sensor arrays into the soft prosthetic hand, we collect a large-scale tactile dataset (including pressure distribution and pressure magnitude) when performing different manipulation tasks. Then, we implement learning-based algorithms to achieve the static object recognition task and the dynamic rolling detection task. In order to achieve the closed-loop control for the soft prosthetic hand, we design a vibrotactile feedback band that is arranged on the upper arm of the user to elicit vibratory stimulation on the skin (Figure 1b). According to the extracted tactile information, the spatial coding feedback strategy is employed to transfer discrimination results to the user by selectively activating vibrotactile motors on the skin. With a set of tests performed by an individual with the transradial amputation and eight able-bodied subjects, we demonstrate that the soft prosthetic hand can help them regain tactile sensation and achieve real-time human-in-the-loop control (Figure 1c) such as finger recognition, diverse object classification, and dynamic rolling direction detection only relying on the tactile feedback with a high accuracy.

2. Results

2.1. Design and Configuration of the Flexible Tactile Sensor Array

We design the flexible piezoresistive tactile sensor array with a multilayer structure to measure the pressure when touching with objects. As illustrated in **Figure 2**a, the piezoresistive tactile sensor array is composed of six layers. A laser-cut force-sensitive film (velostat, 0.1 mm thick) is covered by two layers of metal-plated conductive fabric electrodes (0.05 mm thick). To increase the sensitivity of the sensor unit at low pressure and obtain a stable value of the sensor unit, a hollow polyethylene terephthalate (PET) layer with double-side adhesive is introduced. In addition, two layers of polyacrylate elastomers (VHB 4905, 0.5 mm thick, 3M Very High Bond tape) are utilized to encapsulate the total structure. Depending on the inherent adhesive of the PET layer and VHB layers, all layers can be assembled by means of lamination, resulting in a hierarchical structure. The detailed methods for the fabrication of tactile sensor array can be found in Experimental Section and Figure S1, Supporting Information. Each point of overlap between the top conductive fabric and the bottom conductive fabric is sensitive to the normal force, which causes the electrical resistance to decrease when being pressed (Figure S2, Supporting Information). In addition, the proposed tactile sensor array can be directly integrated on the soft pneumatic actuator. As depicted in Figure 2b, five flexible tactile sensor arrays are evenly arranged on soft finger actuators of the soft hand. With a customized readout circuit (Figure S3, Supporitng Information), we can extract individual sensor measurement by
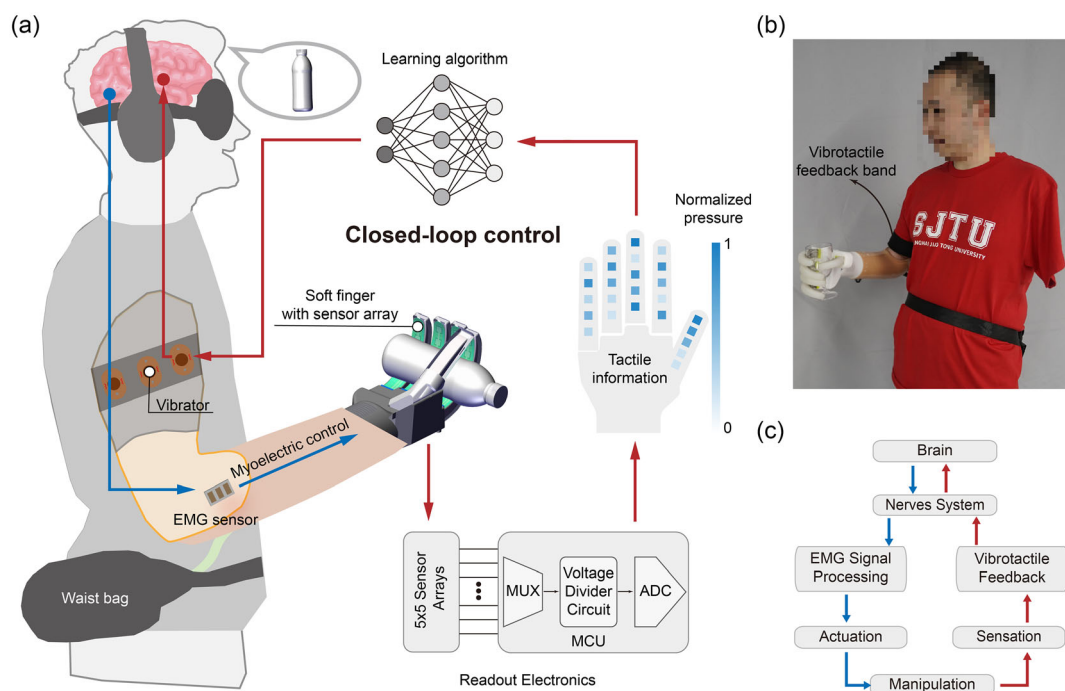

Figure 1. Working principle of the untethered soft prosthetic hand. a) Schematic illustration of the untethered soft prosthetic hand to build a closed-loop control system. b) Photograph of an individual with transradial amputation wearing the soft prosthetic hand. c) Diagram of the human-in-the-loop control of the soft prosthetic hand.
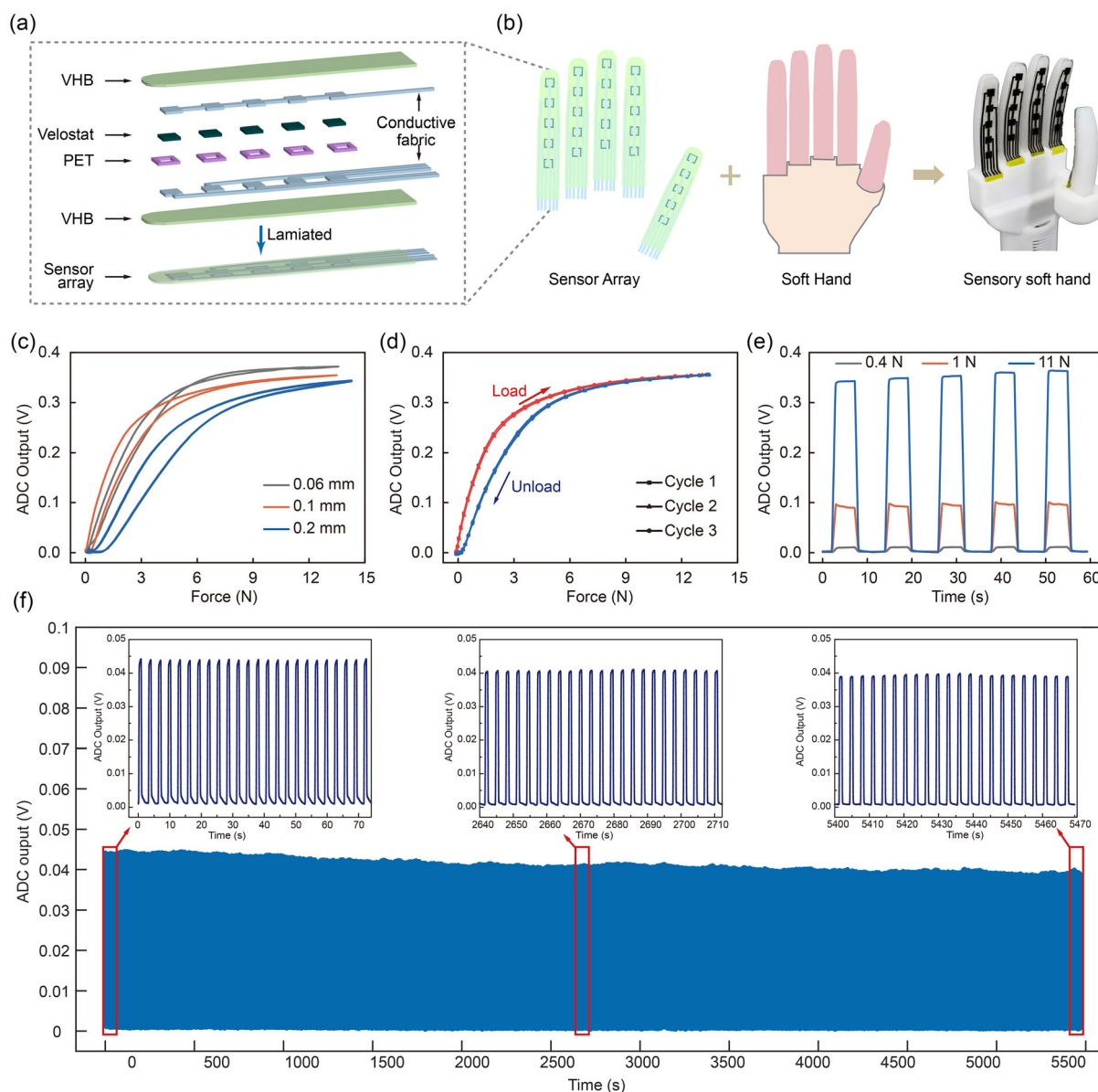
Figure 2. Structure design and performance characterization of the flexible piezoresistive tactile sensor array. a) Exploded-view schematic illustration of the tactile array. b) Integration of the soft hand and tactile sensor array. c) Response of the piezoresistive tactile sensor unit with various thicknesses of the PET layer. d) Loading and unloading response of the piezoresistive tactile sensor unit. e) Response of the piezoresistive tactile sensor unit under periodic loading force of 0.4, 1, and 11 N, respectively. f) Cycling stability at a force of 0.8 N ($\approx$5500 s). The insets show the first 70 s cycles, the middle 70 s cycles, and the last 70 s cycles.

means of multiplexing with almost 6 Hz to form a tactile image (Movie S1, Supporting Information). When adding a small battery, all data acquisition, signal process, and computation are performed on board showing the potential to be integrated into a self-contained untethered soft prosthetic hand.

2.2. Sensing Performances of the Flexible Tactile Sensor Array

To characterize the performances of the tactile sensor, we build an experimental setup (Figure S4a, Supporting information) to

evaluate the electrical and mechanical characteristics of the tactile sensors. A series of tactile sensor arrays are fabricated with different thicknesses of the PET layer (i.e., 0.06, 0.1, 0.2 mm) to investigate the effect on the thickness of the PET layer. The results of the single-tactile sensor unit with different PET layers in typical force response (Figure 2c) reveal that the tactile sensor unit with 0.1 mm PET layer exhibits a higher sensitivity at low-pressure range and has a stable value at high-pressure range. As shown in Figure 2d, the single tactile sensor unit exhibits a sensitivity of $0.06\,\text{V}\,\text{N}^{-1}$ when the force is below 5 N and $0.005\,\text{V}\,\text{N}^{-1}$ in the high force regime of 5–13.6 N with a peak

hysteresis of about 19%, which agree well with the range of grasping force for the soft prosthetic hand.[8] We further explore the force–response capability of the tactile sensor unit. The results (Figure 2e) show that the tactile sensor unit can reflect periodic loads with various forces such as 0.4, 1, and 11 N. Meanwhile, the single-tactile sensor unit exhibits a force–response time of 12 ms and a release time of 13 ms under a low force load ($\approx$0.6 N, Figure S4b, Supporting Information), which is faster than the response speed of the human skin ($\approx$40 ms).[54] For realistic scenario, repeatability is an important index to measure the reliability of the sensor. As shown in Figure 2f, the proposed flexible piezoresistive sensor is subjected to a cyclic loading/unloading force with 0.8 N for a long time ($\approx$5500 s) with little attenuation, revealing a good reliability. In addition, the responses at the loading process of the first stage, the middle stage, and the last stage are magnified to clearly show the reliable durability. We can see that the response curves in different stages are very similar, demonstrating its potential for applications in long-term pressure monitoring scenarios.

2.3. Extraction of Touch Information with Learning-Based Algorithms

Incorporating learning-based algorithm and tactile sensor arrays is an effective way to extract touch information without an explicit model.[55] When achieving diverse manipulation tasks, the output signals of 25 sensor units are normalized (see Experimental Section) and then converted into a 5 × 5 tactile image. As shown in **Figure 3**a, five rows of the tactile image from top to bottom represent the output signals of the sensor units arranged from thumb to pinky and five columns of the tactile image from left to right represent the output signals of the sensor units arranged from tip to root of each soft finger.

For the static classification, we need an accurate and robust learning model. Thus, all different 16 learning models with the same amount of data are evaluated based on their accuracy. Notably, the logistic regression (LR) algorithm[56] is selected because of its high computation accuracy as shown in Figure 3b. To prevent overfitting, L2 regularization is applied during the optimization process and the L2 ratio is set as 5. The classification accuracy of the LR classifier begins convergent and remains stable after around 2400 training data being utilized (Figure 3c).

To achieve the dynamic classification task, such as rolling direction detection, we use a long short-term memory (LSTM) recurrent neural network. LSTM can classify the time series data and have feedback connections to process sequences of data, which makes it suitable for classifying dynamic motions.[57,58] Before transferring to the LSTM layer, we first implement a layer of deep convolutional neural network (CNN) to extract spatial information among adjacent sensors. Then, we use a two-layer multilayer perceptron (MLP) to fully connect them.

Except for the learning-based algorithms, a large-scale tactile dataset with high dimension is also important to reveal tactile information. The integration of high-density sensor units can further enhance the recognition accuracy. Figure 3d demonstrates the classification results when using the dataset from the different numbers of sensor units in each finger. The results show that the low density of sensor units cannot achieve a high classification accuracy. The total classification accuracy using fingers integrated with one sensor unit is about 33.33%. In contrast, high-density sensor units (i.e., five units on each finger) can achieve high static classification (93.33%).

2.4. Application

2.4.1. Untethered Soft Prosthetic Hand System

To help the user restore tactile sensation with prosthetic hand, a soft hand and a wearable feedback band is introduced to
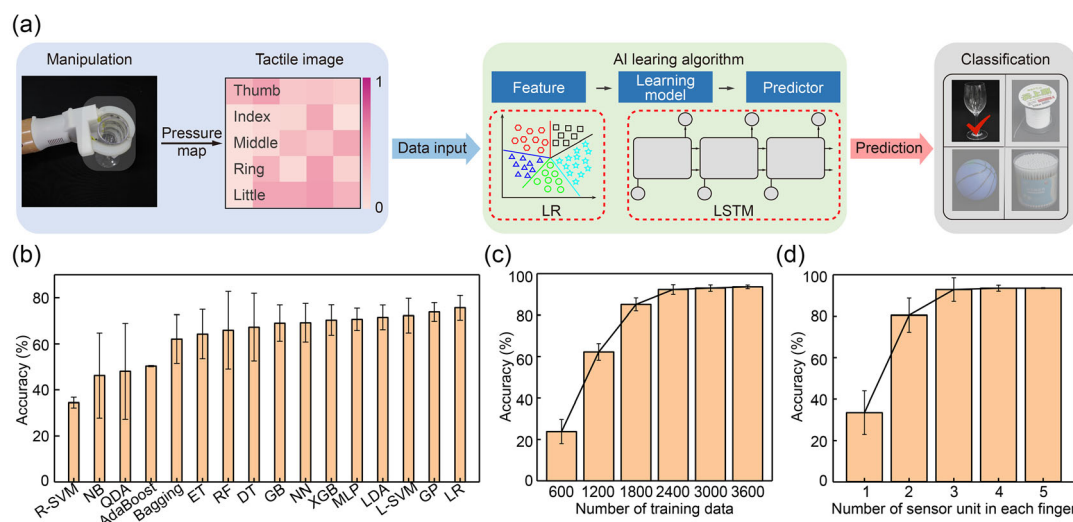

Figure 3. Extraction of touch information from tactile sensor arrays of the soft prosthetic hand. a) Schematic process flow from tactile sensor information collection to real-time learning-based prediction in soft prosthetic hand. b) Classification accuracy of the test sets on all 16 machine learning algorithms. c) The relationship between the number of training data and classification accuracy. d) Comparison of the classification accuracy when using the different densities of sensor units in each finger.

demonstrate the in-future prosthetic hand application. The soft hand consists of five fingers with fiber-reinforced soft elastomeric actuators[8] to mimic the bending movement of the human finger and a 3D printed palm skeleton in the shape of the human palm. Five soft fingers integrated with flexible tactile sensor arrays are mounted on a 3D-printed plastic palm (Imagine 8000) in the shape of a human palm. Then the palm skeleton is connected into a customized plastic socket[8] which is specifically designed for the individual with a transradial amputation according to the shape of his residual limb. In the socket of the prosthetic hand, we implement two Electromyography (EMG) sensors (Danyang prosthetic Factory Co., Ltd) and adopt direct EMG control for the sake of reliability, robustness, and practicality.[9] The output direct-current EMG signals (Figure S5, Supporting Information) are used to decode two kinds of actions (gesture opening and gesture closing) based on the threshold control strategy.[59,60] The decoded motion intention will be used to control the soft prosthetic hand to deliver preset grasping types (See Note S1, Supporting Information). Based on our modular design,[8] all the components of the soft prosthetic hand can be contained in a small bag on the waist of the user. To evaluate the sensing capability of the soft prosthetic hand after integrated tactile sensor arrays, we use the soft hand (at 80 kPa pneumatic pressure to the 1 DOF finger) to grasp a series of objects while measuring the response of the tactile sensor array when interacting with objects. The output of the sensor unit through the analog-to-digital converter (ADC) is linear with respect to the interaction (Figure S6, Supporting Information). After integrating flexible piezoresistive sensory arrays into the soft prosthetic hand, we use the same soft prosthetic hand to build the large-scale tactile dataset and demonstrate the restoring tactile sensation in both static and dynamic tasks. The whole process lasts almost four months, which also indicates the excellent reliability of our untethered soft prosthetic hand. The comparison of some performances such as density of sensor units between our work and recently reported soft hand system is shown in Table S1, Supporting Information.

To convey the tactile sensation, we design a wearable vibrotactile feedback band to inform the user of the touch information through the waveforms created from the vibrotactile motor (Figure S7a, Supporting Information). The vibrotactile feedback band contains five vibration units. Each unit consists of a 3D-printed soft plastic spacer and a vibrotactile motor (10 mm diameter, 2.7 mm height, 0.9 g weight, Figure S7b, Supporting Information). The activation voltage is kept constant at 3 V, which causes a vibration frequency between 150 and 200 Hz. When working at applied voltage (3 V), the mechanical noise of the vibrotactile motor is below 28 dB, which will not be uncomfortable to the user. The acceleration of the generated vibration is 30 m s^{-2}, which means that the users can feel the vibration within 0.02 ms, showing an excellent responsivity. The vibrotactile motor can run continuously for 96 h in an environment from −20 to 60 °C, which indicates good endurance. All five vibration units are uniformly arranged on a sport band with the distance of ≈45 mm. This allows the subject to discriminate touching information using spatial discrimination. Our vibrotactile feedback band provides a light amount of passive squeeze to ensure better vibration. According to the recognized results, different vibration patterns are selectively activated on the specific skin of the limb (see Experimental Section and Figure S7b, Supporting Information).

2.4.2. Performance with Static Classification Tasks

To achieve the static classification task based on tactile data, several tactile images are collected during the interaction with different objects over many minutes to build a custom dataset (see Experimental Section). Then, the normalized tactile data are used as the input data of the developed machine learning algorithm. We establish datasets about fingers recognition and grasped objects discrimination (see Experimental Section). An individual with upper limb amputation demonstrates that wearing the soft prosthetic hand with the developed sensor arrays can help the subject to restore some tactile sensations in static classification tasks (**Figure 4**a). Based on the trained model and the spatial coding strategy for five fingers discrimination, the subject wearing the untethered soft prosthetic hand can accurately distinguish which finger is being pressed in a blindfolded and acoustic environment (Figure 4b and Movie S2, Supporting Information). Different locations on each finger are considered and we are not limited to the fingertip compared to the last generation.[8] We use t-distributed stochastic neighbor embedding (t-SNE) to visualize the group of data for fingers discrimination (Figure 4c). Each point on the plot represents the tactile information of one finger-pressed state projected from the 25-D tactile data into 2D. The points of the same category (with the same color) are clustered together, forming roughly six categories of finger pressed states. In addition, the confusion matrix shows that it has a high accuracy of correction (97.33%) in distinguishing individual finger pressed states (Figure 4d).

To expand the usefulness of the soft prosthetic hand, we operate the hand prosthesis to grasp five standard objects with different sizes and shapes. Notably, different orientations are considered to make it robust. The visualization of the data for objects discrimination using t-SNE is shown in Figure 4e and S8, Supporting Information, shows examples of normalized tactile maps. The extracted features of each finger from grasping these five objects (Figure S9, Supporting Information) also reveal the grasping force of each finger for each object. Then the subject wearing an eye mask and headphones can use his own EMG signals to control the soft prosthetic hand to grasp the selected objects in a random sequence. When the hand firmly grasps the objects, the discrimination results are output and translated into corresponding vibration patterns based on the previous coding method. After receiving the vibration stimulation, the subject will intuitively control the soft prosthetic hand open to achieve the closed-loop control. The results (Figure 4f and Movie S3, Supporting Information) demonstrate that the subject can distinguish five standard objects with an accuracy of 96%.

2.4.3. Performance with the Dynamic Discrimination Task

The human hand has the ability to detect not only static classification task (i.e., object classification) but also dynamic discrimination task (i.e., motion direction detection).[1,2] By programming the sequential activation sequence of the vibrators located in the vibrotactile feedback band, we also demonstrate
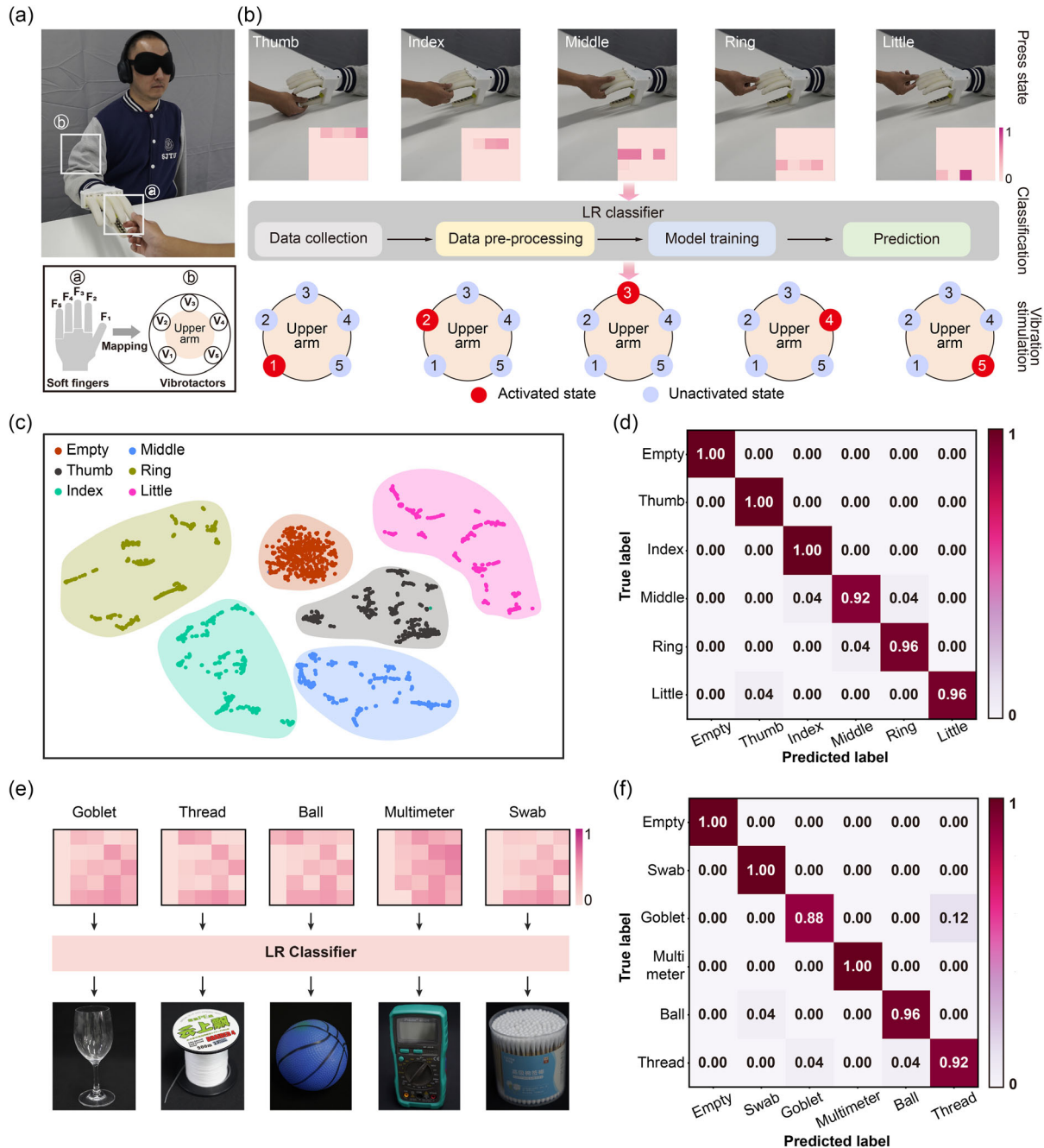
Figure 4. An individual with a transradial amputation wearing the soft prosthetic hand, restoring the static classification function. a) Photographs of the individual with a transradial amputation achieve static classification task. b) Demonstration of restoring the tactile sensation of an individual finger being pressed. c) Visualizing the tactile information in the finger-pressed state dataset using t-SNE dimensionality reduction. The separation of clusters corresponding to each state illustrates the discriminative capability of the tactile sensor array. d) The confusion matrix of the individual finger discrimination with an accuracy of 97.33%. e) Demonstration of restoring the tactile sensation of objects discrimination. f) The confusion matrix of the objects discrimination with an accuracy of 96%.

that the subject wearing the soft prosthetic hand can discriminate the cylinder object rolling directions in the blindfolded and acoustically shielded environment (**Figure 5**a and Movie S4, Supporting Information). In this test, we first use a cylinder (40 mm) to rotate on the hand with two directions (rolling forward and rolling backward, Figure 5b) and collect the response

of the tactile sensor arrays at the same time. Then a dynamic rotation dataset is established based on the normalized tactile data and their corresponding rotation directions (see Experimental Section). We use the deep learning algorithms that contain deep CNN, LSTM, and two-layer MLP based on the PyTorch framework to discriminate dynamic rolling directions
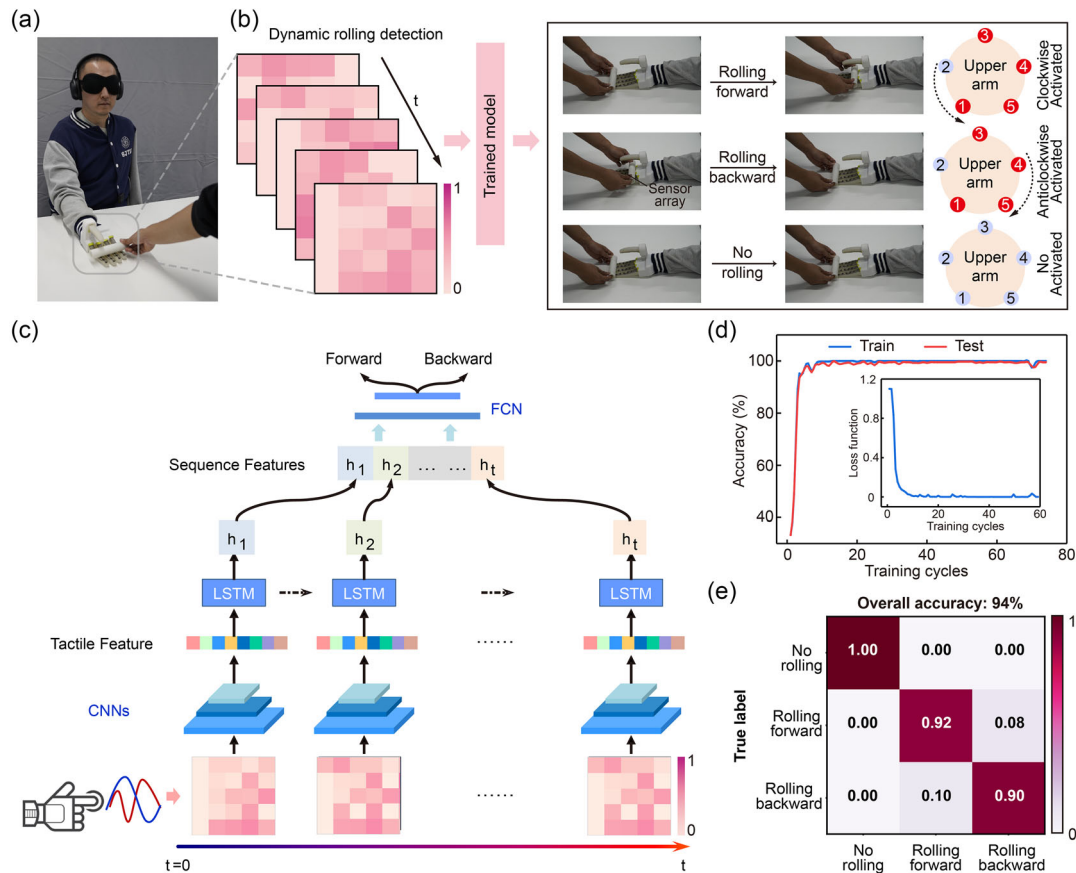
Figure 5. An individual with a transradial amputation wearing the soft prosthetic hand, restoring the dynamic discrimination. a) Photographs of the individual with a transradial amputation achieve dynamic discrimination task. b) Demonstration of restoring the tactile sensation of rolling direction detection. c) The neural network architecture used for restoring the dynamic discrimination from tactile information (5 × 5 arrays). d) The change in classification accuracy of the neural network with the increase of training cycles. e) The confusion matrix of the dynamic rolling discrimination with an accuracy of 94%.

(Figure 5c, Note S2, Supporting Information). The discrimination accuracy of the optimized learning architecture begins convergent and remains stable after 15 training cycles for both training and testing datasets (Figure 5d). Finally, the amputee subject wearing the soft prosthetic hand can well discriminate dynamic rolling directions with a high accuracy of 94% (Figure 5e).

3. Discussion

In this article, we report a flexible tactile sensor array which can be integrated into an untethered soft prosthetic hand to help the transradial amputee subject restore tactile sensation and improve object recognition. The developed flexible piezoresistive sensor arrays including 25 tactile sensor units are conformally integrated on each finger. In this sense, the soft prosthetic hand can detect tactile information such as pressure magnitude and pressure distribution when grasping objects. To reveal the correspondences between tactile information and object attribute while interacting with touched objects, we implement learning-based algorithms. Combined with the EMG-decoding

algorithm and the vibrotactile feedback, eight able-bodied subjects and an individual with transradial amputation cannot only intuitively control the soft prosthetic hand to achieve grasping tasks but also can restore finger tactile sensation and discriminate the grasped objects in a blindfolded and acoustically shielded environment. We have also experimentally demonstrated that the subjects can achieve a dynamic discrimination task such as discriminating the rolling direction of a cylinder. To further improve the sensation performance, a higher density of tactile sensor unit and the multimodal sensor would be integrated into this untethered soft prosthetic hand. For more realistic applications, advanced learning algorithms and more real feedback strategy still need to be investigated.[20,43] We anticipate that this work will accelerate the application of soft prosthetic hands for amputees in daily activities.

4. Experimental Section

Fabrication of the Flexible Piezoresistive Tactile Sensor Array: The fabrication process of the flexible piezoresistive tactile sensor array is illustrated in Figure S1, Supporting Information. The velostat (3M Velostat electrically

**ADVANCED
SCIENCE NEWS**

www.advancedsciencenews.com

**ADVANCED
INTELLIGENT
SYSTEMS**
Open Access

www.advintellsyst.com

conductive copolymer 0.1 mm thick; Adafruit Industries) served as the sensing layer and was cut to evenly fit a soft finger by a laser-cut machine (VLS3.50, Universal Laser Systems, Inc., USA, Figure S1a, Supporting Information). To avoid movement of the velostat layer in the laser-cutting process, a thin layer water was introduced to attach the velostat layer to an acrylic board. Then, the laser-cut sensing layer was washed to remove debris from the surface. The laser-cut conductive fabric (fabric plated with copper and nickel, shier Co. Ltd., China) was arranged on either side of the sensing layer, ensuring that there was no contact between electrodes. Notably, to increase the sensitivity of the sensor at low-pressure range, a laser-cut hollow PET layer with double-side adhesive was used between the sensing layer and the bottom electrode. The overlap region between the top and bottom electrodes could respond to force through a change in the resistance of the sensing layer. Two layers of VHB were laser cut with finger structure for encapsulation. All layers were laminated depending on the inherent adhesive of the PET layer and VHB layers (Figure S1b, Supporting Information). Finally, the conductive fabric was connected to copper wires through thermal welding two layers of weft-knitted polyester fabric coated with TPU (Figure S1c, Supporting Information). The fabric-encapsulated conductive electrodes were connected to the readout circuit. Using the thermal welding process to connect the conductive fabric to copper wires resulted in a robust electrical contact, which is of great significance for long-term use.

Characterization of the Tactile Sensing Arrays: We conducted a series of tests to investigate the mechanical and electrical properties of the tactile sensor array. The experimental setup is shown in Figure S4a, Supporting Information. A stepping motor-driven stage (HST-200, OptoSigma Inc., Japan) equipped with a force gauge (LSB205, Futek Advanced Sensor Technology Inc., USA) at the end was used to apply uniformly normal force. The applied load was controlled at a specific strain rate for different tests (0.002–0.005 m s^{-1}). During the experiment, both the force value and the sensor output were collected using a real-time control board (DS1103, dSPACE Inc., Germany) with 16-bit ADCs.

Assembly of the Soft Prosthetic Hand: We used a surface-treating agent (Ausband 770, xinnuotai Co. Ltd., China) to activate silicon surfaces of the soft finger for the robust bond with the VHB elastomer surface of the tactile sensor array. Then the tactile sensor array and the soft finger were glued together using the liquid elastomer (weiligu Co. Ltd., China). After curing for about 12 h at room temperature, the tactile sensory array and the soft finger were perfectly aligned. Furthermore, five soft fingers after integrated tactile sensory array were installed into the 3D-printed photosensitive–resin palm skeleton (Imagine 8000, SOMOS Inc., Netherlands) through the threaded connection.

Data Acquisition and Normalization Process: The signal of each tactile sensor unit on the soft prosthetic hand was sampled by an ADC converter after being conditioned by the multiplexer circuit (Figure S3, Supporting Information) and then sent to a credit card-sized board (up core plus, yanyang Co. Ltd., China) through COM (cluster communication port) for processing. Each set of tactile data contains 25 signal values of 5 tactile sensor arrays integrated on the soft hand. Then the measured signal of each sensor unit was normalized to 0 to 1. Specifically, normalization was carried out by taking the maximum value of quantity as 1 and the minimum value as 0. We defined 25 normalized signal values from five sensor arrays as a set of data. In discriminating finger press state, we pressed each finger in different locations for some minutes and the tactile responses were collected simultaneously. Due to the higher density of tactile sensor unit compared to our previous work,[8] the press region was not limited to the fingertip. The total dataset was required through pressing finger about 360 times and each group contained 10 sets of tactile data. In discriminating 5 daily objects, the total dataset was required through grasping these objects with different orientations and locations about 360 times and each group contained 10 sets of tactile data. In discriminating dynamic rolling direction, the total dataset was required through rolling the cylinder in different directions about 1500 times and each group contained 1 set of tactile data. The training and testing datasets were randomly selected from the total dataset. To prevent overfitting, the dataset was randomly divided into a training set, a validation set, and a test set at a ratio of 7:2:1. Besides, the training process was terminated when the lost function evaluated by the validation set stopped decreasing for ten training epochs.

Experiments with Human Subjects: All experiments were conducted in accordance with the declaration of Helsinki and approved by the Ethics Committee of Human and Animal Experiments of Shanghai Jiao Tong University. The individual with transradial amputations who participated in this study was recommended by Shanghai Liankang Prosthetics and Orthotics Manufacturing. The able-bodied subjects were recruited from Shanghai Jiao Tong University. The participants did not have any previous neuromuscular disorders and were informed about the experimental procedure and signed the informed consent forms before participation. The authors affirmed that human research participants provided written informed consent for the experimental procedure and publication.

The Training Process for Tactile Feedback: In the training process for tactile feedback, the vibration was activated repeatedly for three periods. Each period consisted of 5 s vibration and 3 s interval. During the training process, we first activated the vibrotactile motor from one to five in sequence for five times to let the subject remember the location and the feeling of the stimulation. The frequency and amplitude of stimulation were the same for all vibrotactile motors involved in the experiments. The subject was told to learn the five vibration sites for five discrimination targets. Then, we activated the vibrotactile motor in a random order to check whether the subject can discriminate the activated vibrotactile motor on the basis of the vibration stimulation. In the discriminating finger press state, the vibrotactile motors from 1 to 5 corresponded from thumb to pinky. In discriminating five daily objects, the five vibrotactile motors from 1 to 5 corresponded to goblet, thread, ball, multimeter, and swab. The training process lasted about 10 min. In the discriminating dynamic rolling direction, we activated the vibrotactile motors in a sequence (i.e., clockwise activated and anticlockwise activated) to map different rolling directions. During each sequence, each vibrotactor was activated for 4 s and the adjacent vibrotactor was also activated before the vibration of the previous vibrotactor finished (1 s ahead). Eight able-bodied subjects were recruited to test the spatial coding method. All subjects were blindfolded and acoustically shielded to eliminate visual and auditory feedback interference. Results (Figure S10–S12, Supporting Information) showed that all subjects could achieve both static and dynamic discrimination tasks relying on the vibrotactile feedback with high accuracies. The reason causing the final classification error consisted of model error in the model prediction stage and cognitive error from vibrotactile feedback in the feeling of vibration stimulation stage. Surfaces of grasped objects such as swab, goblet, and thread were all nearly cylindrical, which resulted in similar tactile images. This similarity may lead to prediction errors when the learning-based model was trained without huge dataset. Although prediction errors exist, we believed that the classification accuracy ($>95\%$) was sufficiently high for daily applications. In our future work, we will employ two methods to correct these prediction errors: one is to create a larger training dataset, such as repeatedly collecting data with various grasping positions for more days, and the other is to utilize more powerful neural networks, such as autoencoders and attention-based CNNs.

Supporting Information

Supporting Information is available from the Wiley Online Library or from the author.

Acknowledgements

**ADVANCED
SCIENCE NEWS**

www.advancedsciencenews.com

**ADVANCED
INTELLIGENT
SYSTEMS**
Open Access

www.advintellsyst.com

Conflict of Interest

The authors declare no conflict of interest.

Data Availability Statement

The data that support the findings of this study are available from the corresponding author upon reasonable request.

Keywords

[1] V. E. Abraira, D. D. Ginty, *Neuron* **2013**, *79*, 618.

[2] A. B. Vallbo, R. S. Johansson, *Hum. Neurobiol.* **1984**, *3*, 3.

[3] L. E. Osborn, M. M. Iskarous, N. V. Thakor, in *Wearable Robotics*, Elsevier, Amsterdam **2020**, pp. 445–468.

[4] J. T. Belter, J. L. Segil, A. M. Dollar, R. F. Weir, *J. Rehabil. Res. Dev.* **2013**, *50*, 599.

[5] F. Cordella, A. L. Ciancio, R. Sacchetti, A. Davalli, A. G. Cutti, E. Guglielmelli, L. Zollo, *Front. Neurosci.* **2016**, *10*, 209.

[6] E. A. Biddiss, T. T. Chau, *Prosthet. Orthot. Int.* **2007**, *31*, 236.

[7] D. Farina, O. Aszmann, *Sci. Transl. Med.* **2014**, *6*, 257ps12.

[8] G. Gu, N. Zhang, H. Xu, S. Lin, Y. Yu, G. Chai, L. Ge, H. Yang, Q. Shao, X. Sheng, X. Zhu, X. Zhao, *Nat. Biomed. Eng.* **2021**, *7*, 589.

[9] M. Laffranchi, N. Boccardo, S. Traverso, L. Lombardi, M. Canepa, A. Lince, M. Semprini, J. A. Saglia, A. Naceri, R. Sacchetti, E. Gruppioni, L. D. Michieli, *Sci. Rob.* **2020**, *5*, eabb0467

[10] P. Capsi-Morales, C. Piazza, M. G. Catalano, G. Grioli, L. Schiavon, E. Fiaschi, A. Bicchi, *Sci. Rep.* **2021**, *11*, 23952.

[11] Vincent Systems, Vincent Hand, https://www.vincentsystems.de/vincent-evolution4?lang=en (accessed: 2022).

[12] Össur, iLimb Ultra titanium, https://www.ossur.com/en-us/prosthetics/arms/i-limb-ultra-titanium (accessed: 2022).

[13] Ottobock, BeBionic Hand, https://www.ottobock.com/en-us/product/8E70 (accessed: 2022).

[14] Ottobock, Michelangelo Prosthetic Hand, https://www.ottobock.com/en-us/product/8E500 (accessed: 2022).

[15] E. D'Anna, G. Valle, A. Mazzoni, I. Strauss, F. Iberite, J. Patton, F. M. Petrini, S. Raspopovic, G. Granata, R. D. Iorio, M. Controzzi, C. Cipriani, T. Stieglitz, P. M. Rossini, S. Micera, *Sci. Rob.* **2019**, *4*, eaau8892.

[16] S. M. Engdahl, B. P. Christie, B. Kelly, A. Davis, C. A. Chestek, D. H. Gates, *J. NeuroEng. Rehabil.* **2015**, *12*, 53.

[17] D. Farina, N. Jiang, H. Rehbaum, A. Holobar, B. Graimann, H. Dietl, O. C. Aszmann, *IEEE Trans. Neural Syst. Rehabil. Eng.* **2014**, *22*, 797.

[18] L. E. Osborn, A. Dragomir, J. L. Betthauser, C. L. Hunt, H. H. Nguyen, R. R. Kaliki, N. V. Thakor, *Sci. Rob.* **2018**, *3*, eaat3818.

[19] K. Gilday, J. Hughes, F. Iida, *Soft Rob.* **2023**, *10*, 159.

[20] Y. H. Jung, J.-Y. Yoo, A. Vázquez-Guardado, J.-H. Kim, J.-T. Kim, H. Luan, M. Park, J. Lim, H.-S. Shin, C.-J. Su, R. Schloen, J. Trueb, R. Avila, J.-K. Chang, D. S. Yang, Y. Park, H. Ryu, H.-J. Yoon, G. Lee, H. Jeong, J. U. Kim, A. Akhtar, J. Cornman, T. Kim, Y. Huang, J. A. Rogers, *Nat. Electron.* **2022**, *5*, 374.

[21] C. Laschi, B. Mazzolai, M. Cianchetti, *Sci. Rob.* **2016**, *1*, eaah3690.

[22] B. Shih, D. Shah, J. Li, T. G. Thuruthel, Y.-L. Park, F. Iida, Z. Bao, R. Kramer-Bottiglio, M. T. Tolley, *Sci. Rob.* **2020**, *5*, eaaz9239.

[23] M. Cianchetti, C. Laschi, A. Menciassi, P. Dario, *Nat. Rev. Mater.* **2018**, *3*, 143.

[24] G. Gu, H. Xu, S. Peng, L. Li, S. Chen, T. Lu, X. Guo, *Soft Rob.* **2019**, *6*, 368.

[25] M. Wang, Z. Yan, T. Wang, P. Cai, S. Gao, Y. Zeng, C. Wan, H. Wang, L. Pan, J. Yu, S. Pan, K. He, J. Lu, X. Chen, *Nat. Electron.* **2020**, *3*, 563.

[26] Z. Shen, Z. Zhang, N. Zhang, J. Li, P. Zhou, F. Hu, Y. Rong, B. Lu, G. Gu, *Adv. Mater.* **2022**, *34*, 2203650.

[27] C. M. Boutry, M. Negre, M. Jorda, O. Vardoulis, A. Chortos, O. Khatib, Z. Bao, *Sci. Rob.* **2018**, *3*, eaau6914.

[28] S. Lee, S. Franklin, F. A. Hassani, T. Yokota, M. O. G. Nayeem, Y. Wang, R. Leib, G. Cheng, D. W. Franklin, T. Someya, *Science* **2020**, *370*, 966.

[29] Z. Zhu, R. Li, T. Pan, *Adv. Mater.* **2018**, *30*, 1705122.

[30] X. Pu, M. Liu, X. Chen, J. Sun, C. Du, Y. Zhang, J. Zhai, W. Hu, Z. L. Wang, *Sci. Adv.* **2017**, *3*, 1700015.

[31] X. Qu, Z. Liu, P. Tan, C. Wang, Y. Liu, H. Feng, D. Luo, Z. Li, Z. L. Wang, *Sci. Adv.* **2022**, *8*, eabq2521.

[32] Y. Yan, Z. Hu, Z. Yang, W. Yuan, C. Song, J. Pan, Y. Shen, *Sci. Rob.* **2021**, *6*, eabc8801.

[33] J. Ge, X. Wang, M. Drack, O. Volkov, M. Liang, G. S. Cañón Bermúdez, R. Illing, C. Wang, S. Zhou, J. Fassbender, M. Kaltenbrunner, D. Makarov, *Nat. Commun.* **2019**, *10*, 4405.

[34] T. Kim, S. Lee, T. Hong, G. Shin, T. Kim, Y.-L. Park, *Sci. Rob.* **2020**, *5*, eabc6878.

[35] H. Bai, S. Li, J. Barreiros, Y. Tu, C. R. Pollock, R. F. Shepherd, *Science* **2020**, *370*, 848.

[36] O. A. Araromi, M. A. Graule, K. L. Dorsey, S. Castellanos, J. R. Foster, W.-H. Hsu, A. E. Passy, J. J. Vlassak, J. C. Weaver, C. J. Walsh, R. J. Wood, *Nature* **2020**, *587*, 219.

[37] P. Lu, L. Wang, P. Zhu, J. Huang, Y. Wang, N. Bai, Y. Wang, G. Li, J. Yang, K. Xie, J. Zhang, B. Yu, Y. Dai, C. F. Guo, *Sci. Bull.* **2021**, *66*, 1091.

[38] T. Yao, X. Guo, C. Li, H. Qi, H. Lin, L. Liu, Y. Dai, L. Qu, Z. Huang, P. Liu, C. Liu, Y. Huang, G. Xing, *J. Phys. Appl. Phys.* **2020**, *53*, 445109.

[39] X. Guo, W. Hong, L. Liu, D. Wang, L. Xiang, Z. Mai, G. Tang, S. Shao, C. Jin, Q. Hong, Y. Zhao, Y. Xia, L. Yang, G. Xing, *ACS Appl. Nano Mater.* **2022**, *5*, 11028.

[40] X. Guo, D. Zhou, W. Hong, D. Wang, T. Liu, D. Wang, L. Liu, S. Yu, Y. Song, S. Bai, Y. Li, Q. Hong, Y. Zhao, L. Xiang, Z. Mai, G. Xing, *Small* **2022**, *18*, 2203044.

[41] J. Qiu, X. Guo, R. Chu, S. Wang, W. Zeng, L. Qu, Y. Zhao, F. Yan, G. Xing, *ACS Appl. Mater. Interfaces* **2019**, *11*, 40716.

[42] Z. Shen, X. Zhu, C. Majidi, G. Gu, *Adv. Mater.* **2021**, *33*, 2102069.

[43] S. Sundaram, P. Kellnhofer, Y. Li, J.-Y. Zhu, A. Torralba, W. Matusik, *Nature* **2019**, *569*, 698.

[44] K. Sim, Z. Rao, Z. Zou, F. Ershad, J. Lei, A. Thukral, J. Chen, Q.-A. Huang, J. Xiao, C. Yu, *Sci. Adv.* **2019**, *5*, eaav9653.

[45] R. Zuo, Z. Zhou, B. Ying, X. Liu, in *2021 IEEE Int. Conf. Robot. Autom. ICRA*, IEEE, Piscataway, NJ **2021**, pp. 12164–12169.

[46] L. Osborn, R. R. Kaliki, A. B. Soares, N. V. Thakor, *IEEE Trans. Haptic* **2016**, *9*, 196.

[47] T. R. Makin, F. de Vignemont, A. A. Faisal, *Nat. Biomed. Eng.* **2017**, *1*, 0014.

**ADVANCED
SCIENCE NEWS**

www.advancedsciencenews.com

**ADVANCED
INTELLIGENT
SYSTEMS**

www.advintellsyst.com

[48] O. Blanke, *Nat. Rev. Neurosci.* **2012**, *13*, 556.

[49] H. H. Ehrsson, B. Rosén, A. Stockselius, C. Ragnö, P. Köhler, G. Lundborg, *Brain* **2008**, *131*, 3443.

[50] L. Zollo, G. Di Pino, A. L. Ciancio, F. Ranieri, F. Cordella, C. Gentile, E. Noce, R. A. Romeo, A. Dellacasa Bellingegni, G. Vadalà, S. Miccinilli, A. Mioli, L. Diaz-Balzani, M. Bravi, K.-P. Hoffmann, A. Schneider, L. Denaro, A. Davalli, E. Gruppioni, R. Sacchetti, S. Castellano, V. Di Lazzaro, S. Sterzi, V. Denaro, E. Guglielmelli, *Sci. Rob.* **2019**, *4*, eaau9924.

[51] M. R. Motamedi, J. Roberge, V. Duchaine, *IEEE Trans. Neural Syst. Rehabil. Eng.* **2017**, *25*, 1230.

[52] X. Yu, Z. Xie, Y. Yu, J. Lee, A. Vazquez-Guardado, H. Luan, J. Ruban, X. Ning, A. Akhtar, D. Li, B. Ji, Y. Liu, R. Sun, J. Cao, Q. Huo, Y. Zhong, C. Lee, S. Kim, P. Gutruf, C. Zhang, Y. Xue, Q. Guo, A. Chempakasseril, P. Tian, W. Lu, J. Jeong, Y. Yu, J. Cornman, C. Tan, B. Kim, K. Lee, X. Feng, Y. Huang, J. A. Rogers, *Nature* **2019**, *575*, 473.

[53] S. Dosen, M. Markovic, M. Strbac, M. Belic, V. Kojic, G. Bijelic, T. Keller, D. Farina, *IEEE Trans. Neural Syst. Rehabil. Eng.* **2017**, *25*, 183.

[54] Q.-J. Sun, X.-H. Zhao, Y. Zhou, C.-C. Yeung, W. Wu, S. Venkatesh, Z.-X. Xu, J. J. Wylie, W.-J. Li, V. A. L. Roy, *Adv. Funct. Mater.* **2019**, *29*, 1808829.

[55] G. Li, S. Liu, L. Wang, R. Zhu, *Sci. Rob.* **2020**, *5*, eabc8134.

[56] N. M. Nasrabadi, *J. Electron. Imaging* **2006**, *16*, 049901.

[57] J. DelPreto, J. Hughes, M. D'Aria, M. de Fazio, D. Rus, *IEEE Rob. Autom. Lett.* **2022**, *7*, 710589.

[58] S. Hochreiter, J. Schmidhuber, *Neural Comput.* **1997**, *9*, 1735.

[59] L. Lucas, M. DiCicco, Y. Matsuoka, *J. Rob. Mechatron.* **2004**, *16*, 482.

[60] M. Zecca, S. Micera, M. C. Carrozza, P. Dario, *Crit. Rev. Biomed. Eng.* **2002**, *30*, 459.